Carbon 146 (2019) 447–461

Contents lists available at ScienceDirect

Carbon

journal homepage: www.elsevier.com/locate/carbon

Capacitance-based self-sensing of flaws and stress in carbon-carbon composites, with reports of the electric permittivity, piezoelectricity and piezoresistivity

Xiang Xi, D.D.L. Chung*

Composite Materials Research Laboratory, Department of Mechanical and Aerospace Engineering, University at Buffalo, The State University of New York, Buffalo, NY, 14260-4400, USA

ARTICLE INFO

Article history:
Received 5 November 2018
Received in revised form
7 January 2019
Accepted 19 January 2019
Available online 25 January 2019

ABSTRACT

Capacitance-based nondestructive flaw evaluation (NDE), electric permittivity, piezoelectricity (capacitance-based stress/strain self-sensing) and piezoresistivity (resistance-based stress/strain self-sensing) of carbon-carbon composite (C/C, density 1.5 g/cm^3, PAN-based carbon fiber) are unprecedentedly reported. The in-plane capacitance measured using coplanar electrodes decreases monotonically with increasing cumulative artificially inflicted damage (1–62 blind/through holes, diameter 1.00 mm), indicating NDE feasibility. The in-plane relative permittivity is 1.1×10^4 (2 kHz); the in-plane DC resistivity is 2.4×10^{-3} Ω.cm. These values are similar to those previously reported for PAN-based carbon fiber. The permittivity increases reversibly by up to 16% with increasing elastic tensile strain (up to 0.0081%). However, the contribution of the stress-dependent permittivity to the piezoelectric effect is negligible. The observed in-plane direct piezoelectric effect is primarily due to the reversible monotonic decrease of the electric field output with the increasing tensile strain. The piezoelectric coupling coefficient d_{33} is negative, $-(8.1 \pm 0.2) \times 10^{-9}$ pC/N, in contrast to the positive value of $+(1.7 \pm 0.3) \times 10^{-8}$ pC/N for PAN-based carbon fiber. The in-plane piezoresistivity gage factor is negative, -7804 ± 429, which is much higher in magnitude than -1830 ± 47 previously reported for PAN-based carbon fiber. The differences in d_{33} and gage factor between C/C and PAN-based carbon fiber are attributed mainly to the carbon matrix in the C/C.

1. Introduction

Carbon-carbon composites (continuous carbon fiber carbon-matrix composites) (abbreviated C/C) are the dominant structural materials for high-temperature lightweight structures, as needed for missiles, missile launchers, space reentry vehicles, aircraft brakes, etc. [1–9]. The detection of the flaws such as delamination in these materials is critically needed for the safety and effective operation of various strategic structures. In addition, the detection of the flaws at various stages of the expensive fabrication process of these composites (involving multiple cycles of densification) is important, as the presence of flaws at a certain stage of the fabrication may indicate that it is not worthwhile to continue with the subsequent expensive steps of densification. Therefore, nondestructive evaluation (NDE) of the composites is needed both during the composite fabrication and during the use of the material.

Current NDE methods have various inadequacies. Eddy current inspection is not suitable, due to the inadequate conductivity of carbon-carbon composites. X-ray tomography is inadequate for detecting small flaws and is not amenable to inspection in the field. Ultrasonic inspection requires well-defined cracks that can reflect the incoming ultrasonic wave, in addition to requiring the movement of a transducer over the surface of the material under inspection. This movement may not be feasible over obscured regions of the surface, such as regions obscured by joints (e.g., fastened joints) or coatings (e.g., oxidation protection layers, dirt, reaction products, etc.). Even if the movement over the obscured region is feasible, the obscuring object may render the sensing of the material underneath it ineffective, particularly if the object is non-uniformly distributed over the surface of the material under evaluation. In addition, the movement requires a smooth surface.

* Corresponding author.
E-mail address: ddlchung@buffalo.edu (D.D.L. Chung).
URL: http://alum.mit.edu/www/ddlchung

https://doi.org/10.1016/j.carbon.2019.01.062
0008-6223/

For the inspection of C/C, reported methods include ultrasonic methods [10,11], acoustic emission [12], infrared thermography [13–17], X-ray computed microtomography [18], digital image correlation [19] and electrical resistance measurement [20,21]. X-ray computed microtomography is not suitable for inspection in the field. Acoustic emission is effective for detecting damage while the damage is being inflicted. Digital image correlation involves examining the surface using a camera and is not effective for sensing internal defects that do not affect the surface topography. Infrared thermography gives the temperature distribution through detecting the infrared emission, which is not adequately sensitive to defects, particularly after the damage infliction.

Electrical measurements are attractive in their fast response and the portability of the measurement meters. The measurement of the electrical resistance has been previously reported to be effective for sensing the damage in C/C [20,21]. Damage increases the resistance. However, resistance measurement requires electrical contacts (electrodes) that are in intimate contact with the material under evaluation, so that the resistance associated with the contacts is not significant. The use of four electrical contacts (i.e., the four-probe method), with the outer two contacts for passing current and the inner two contacts for measuring the voltage, is effective for essentially removing the contribution of the contact resistance from the measured resistance [22]. However, the installation of four contacts (as opposed to two contacts) complicates the implementation of the technology in a structure, particularly if the structure is not simple in shape and the resistivity distribution (which relates to the damage distribution) is to be determined. Furthermore, the silver paint used in the prior work [20] and other conductive pastes applied at the interface between the electrode and the surface of the material under evaluation [23] are not capable to withstand the high temperatures at which C/C are typically used. Another type of electrical contact is in the form of pressure contacts, which provide electrical contact between two surfaces by using pressure without the use of a conductive paint or paste between the two surfaces. Pressure contacts tend to be associated with high contact resistance compared to the use of a conductive paint or paste. This is because no surface is perfectly flat and the contacting surfaces in a pressure contact touch one another at points only [24-26]. In case that the C/C is covered by a low-conductivity coating, such as a silicon carbide coating that is commonly used for oxidation protection, the local removal of the coating is necessary prior to the application of the electrical contacts. The coating removal is inconvenient and tends to degrade irreversibly the performance of the C/C (such as the decrease of the oxidation protection).

Resistance and capacitance are two attributes of the electrical behavior. Another type of electrical measurement involves measuring the capacitance rather than the resistance. In contrast to resistance measurement, capacitance measurement does not require the electrical contacts to be intimate and requires only two electrical contacts. In case that the material under evaluation is conductive (as in the case of C/C), the capacitance measurement needs to be made with the presence of a dielectric film positioned between the contact and the material under inspection [27]. The need for a dielectric film stems from the fact that an LCR meter is not designed for measuring the capacitance of a low-resistance material system. The importance of the dielectric film has been shown by the large difference in capacitance reading between measurements with and without a dielectric film in case of reduced graphite oxide [28]. Although adhesive tape (which is not resistant to high temperatures) is used as the dielectric film in the prior work [27], ceramics or other high temperature materials can be used instead as the dielectric film.

Capacitance measurement has been recently shown to be effective for the NDE of continuous carbon fiber polymer-matrix composite (abbreviated CFRP) [27]. Judiciously positioned artificial damage (1.1-mm diameter through-holes) causes the in-plane capacitance (as measured using two coplanar electrodes) to decrease monotonically, due to the effect of the damage on the fringing electric field emanating from the electrodes to the parts of the composite away from the electrodes [27].

Carbon-carbon composites tend to be more conductive than carbon fiber polymer-matrix composites, due to the high conductivity of the carbon matrix compared to that of the polymer matrix. The conductivity affects the current spreading, i.e., the spreading of the fringing electric field. This work is directed at investigating for the first time the use of capacitance measurement for sensing the damage and stress/strain in C/C. The sensing of stress/strain is valuable for structural vibration control, load monitoring and structural operation control.

The use of either capacitance or resistance measurement to sense the condition of a structural material means that the sensing is achieved without any embedded or attached sensor. Electrical contacts applied to the material are not sensors. This is known as structural self-sensing, as the structural material senses itself. Compared to the use of embedded or attached sensors, self-sensing is advantageous in the low cost, high durability, last sensing volume and the absence of mechanical property loss.

The capacitance is governed by the electric permittivity, which is a material property. Therefore, this work is also directed at investigating for the first time the permittivity of C/C. Prior work has reported the permittivity of CFRP [27].

The piezoelectric behavior and electric permittivity are related, as both involve the electric polarization of the material. The piezoelectric behavior is useful for sensing strain/stress/damage through the use of the direct piezoelectric effect, which converts mechanical energy to electrical energy. It can also be useful for mechanical energy harvesting. The inherent piezoelectric behavior of C/C has not been previously reported, and should be distinguished from piezoelectric behavior provided by embedding or attaching a piezoelectric device. Therefore, this work is directed at investigating for the first time the inherent piezoelectric behavior of C/C.

The conductivity and permittivity are two aspects of the electrical behavior of a material. In order to shed more light on the electrical behavior, this work includes investigation of the electrical resistivity and piezoresistivity of C/C. Piezoresistivity refers to the effect of strain or stress on the electrical resistivity and is useful for resistance-based sensing. Piezoresistivity has been previously reported for CFRP [29], but has not been previously reported for C/C.

2. Basic concepts

2.1. Piezoelectricity

The direct piezoelectric effect is associated with the change in polarization ΔP due to a change in stress. It is given by Ref. [30].

$$\Delta P = (\kappa - 1)(\Delta Q/A) + (\Delta\kappa)(Q/A) + \Delta\kappa\,\Delta Q/A, \quad (1)$$

Where ΔQ is the change in the stored charge due to the change in stress $\Delta\sigma$, $\Delta\kappa$ is the change in κ due to the change in stress, κ is the relative permittivity in the absence of the change in stress, Q is the stored charge in the absence of the change in stress, and A is the area of the capacitor. The first term on the right side of Eq. (1) describes the well-known piezoelectric effect, which is due to the change in Q; the second term describes the less well-known piezoelectric effect that is due to the change in κ; the third term describes an even less well-known piezoelectric effect that is due to

both the change in κ and the change in Q. Eq. (1) means that the polarization changes in response to both the change in Q and the change in κ. The piezoelectric coupling coefficient d (i.e., d_{33}) is defined by

$$d = \Delta P/\Delta\sigma. \quad (2)$$

If the piezoelectric effect were only due to the change in Q (i.e., the first term on the right side of Eq. (1)), d is given by Ref. [30].

$$d = (\kappa - 1)\,\varepsilon_o\,\Delta E/\Delta\sigma, \quad (3)$$

Where ΔE is the change in electric field due to the change in stress $\Delta\sigma$, as given by the slope of the designated relatively linear part of the curve of ΔE vs. $\Delta\sigma$.

If the piezoelectric effect were only due to the change in κ (i.e., the second term on the right side of Eq. (1)),

$$d = (\Delta\kappa)\,(Q/A)\,/\,\Delta\sigma = (\Delta\kappa\,/\Delta\sigma)\,\varepsilon_o E, \quad (4)$$

Where E is the electric field in the absence of the change in stress, and $\Delta\kappa$ is the change in κ due to the change in stress $\Delta\sigma$, as given by the slope of the designated relatively linear part of the curve of $\Delta\kappa$ vs. $\Delta\sigma$.

If the piezoelectric effect were only due to the last term on the right side of Eq. (1),

$$d = (\Delta\kappa\,/\Delta\sigma)\,\varepsilon_o\,\Delta E, \quad (5)$$

Where ΔE is the change in electric field due to the change in stress $\Delta\sigma$.

2.2. Piezoresistivity

Piezoresistivity refers to the change in resistivity with strain, which relates to the stress. It is to be distinguished from the change in resistance due to the dimensional changes resulting from the strain or stress. Unless the strain results in a degree of damage or irreversible microstructural change, piezoresistivity is a reversible effect.

The fractional change in resistance ($\delta R/R$) relates to the fractional change in resistivity ($\delta\rho/\rho$), the longitudinal strain ($\delta\ell/\ell$) and the Poisson's ratio (ν) according to the equation [30].

$$\delta R/R = \delta\rho/\rho + (\delta\ell/\ell)(1 + 2\nu), \quad (6)$$

For the case in which the material is isotropic in the two transverse directions, i.e., $\nu_{12} = \nu_{13}$. For the resistance in an in-plane direction of C/C, the material is not isotropic in the two directions that are transverse to the resistance direction. However, due to (i) the scarcity of C/C Poisson's ratio data in the literature and (ii) the small value of the reported ratio of 0.073 [31] causing the contribution of the Poisson's ratio term to $\delta R/R$ in Eq. (6) small, this work assumes the validity of Eq. (6).

The gage factor, which is defined as the fractional change in resistance per unit strain, is a widely used way of describing of the extent of piezoresistivity. For a strain sensor that is not piezoresistive, but provides strain sensing due to the effect of the dimensional changes alone on the resistance, the gage factor is about 2, with the exact value depending on the Poisson's ratio ν. The gage factor can be calculated based on Eq. (6), with the extent of the change in $\delta\rho/\rho$ with the stress obtained from the initial slope of the curve of $\delta\rho/\rho$ vs. stress, and the strain obtained by dividing the measured stress by the known elastic modulus, provided that the deformation is in the elastic regime. This work concerns only small strains in the elastic regime, which is the dominant regime of deformation anyway.

3. Experimental methods

3.1. Materials

The C/C is a biaxially woven carbon fiber carbon-matrix composite kindly provided by SGL Carbon, St. Marys, PA, as SIGRABOND C/C. The carbon fiber is based on polyacrylonitrile (PAN). The structure is shown by the optical microscope images in Fig. 1. According to the manufacturer, the density is 1.5 g/cm^3; the flexural strength is 150 MPa; the flexural modulus (comparable to the tensile modulus [32]) is 60 GPa; the tensile strength is 350 MPa; the interlaminar shear strength is 8 MPa; the in-plane electrical resistivity at room temperature is 2.4×10^{-5} Ω .m; the ash content is 1000 ppm; and the maximum application temperature is 2000 °C in vacuum or inert gas. The specimen size is 8 in (203.2 mm) × 6 in (152.4 mm) × 1.40 mm. The Poisson's ratio is taken to be 0.073 [31]. All testing is conducted along one of the two fiber directions of the composite.

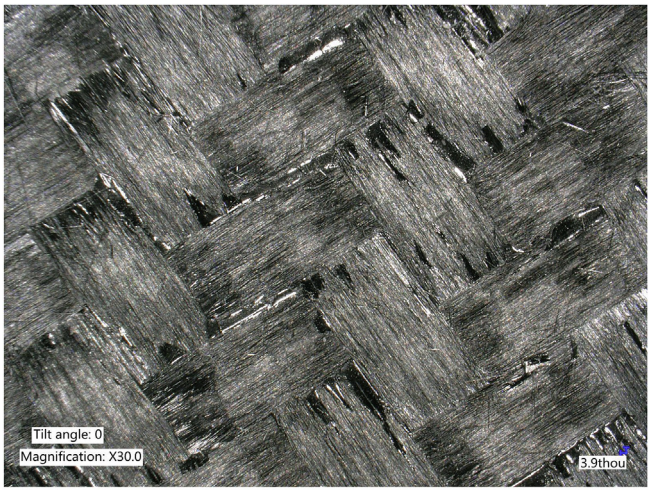

(a)

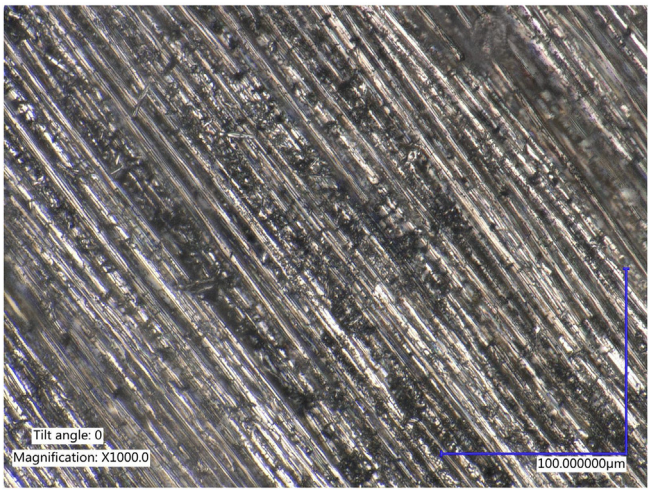

(b)

Fig. 1. Optical micrographs of carbon-carbon composite. The vertical and horizontal scale bars are the same. (a) Low magnification view of the fabric. The short scale bar has length 99 µm (0.0039 inch). (b) High magnification view of a part of a tow in the fabric. The long scale bar has length 100 µm.

3.2. Mechanical testing method

The mechanical testing system is stepper motor-driven (Mark-10 ESM303, Mark-10 Corp., Copiague, NY), providing tensile force up to 1.5 kN. The force is increased at the rate 90 N/min. The tensile stress is given by the force divided by the cross-sectional area of 12,000 fibers. The specimen is a rectangular strip, with the long direction along the direction of capacitance or resistance measurement. It is gripped at its two ends with the help of adhesively bonded cardboard end tabs. The highest stress is 4.82 MPa, which is very small compared to the tensile strength of 350 MPa. Thus, the deformation is in the elastic regime.

3.3. Permittivity and capacitance measurement methods

The method of permittivity measurement is an extension of the method of prior work for continuous carbon fiber polymer-matrix composite [27], steel [33], aluminum [34] and copper [35]. It involves a dielectric film between the specimen and each electrode. The method also involves the decoupling of the interfacial capacitance from the volumetric capacitance, as explained below. In this context, the interface is that between the specimen and electrode, including the dielectric film. The specimen is a rectangular strip, with the long direction along the direction of capacitance measurement.

For decoupling the interfacial capacitance from the volumetric capacitance, four electrodes in the form of aluminum foil are positioned on the top surface of the specimen at four points (essentially equally spaced at a distance of ~63.51 mm, with the exact value measured for each specimen) along the length of the specimen (Fig. 2). Each electrode is adhered to the top surface of the specimen by using 6 layers of double-sided adhesive tape (thickness 0.462 mm for the 6 layers combined), which serves as the dielectric film. Each electrode is 3.18 mm wide in the direction of the length of the specimen, such that it extends all the way along the 15.35-mm width of the specimen. By using different pairs of electrodes (the 1st and 2nd, the 1st and 3rd, and the 1st and 4th), measurement of the capacitance is conducted over distances of L (~63.51 mm), $2L$ (~127.01 mm) and $3L$ (~190.51 mm), with the exact values measured for each specimen.

The capacitance is measured using an LCR meter (Instek LCR-816 High Precision LCR Meter). The frequency is 2.000 kHz, because this is the highest frequency provided by the meter and a frequency in the kHz range is commonly available and widely used. The error in

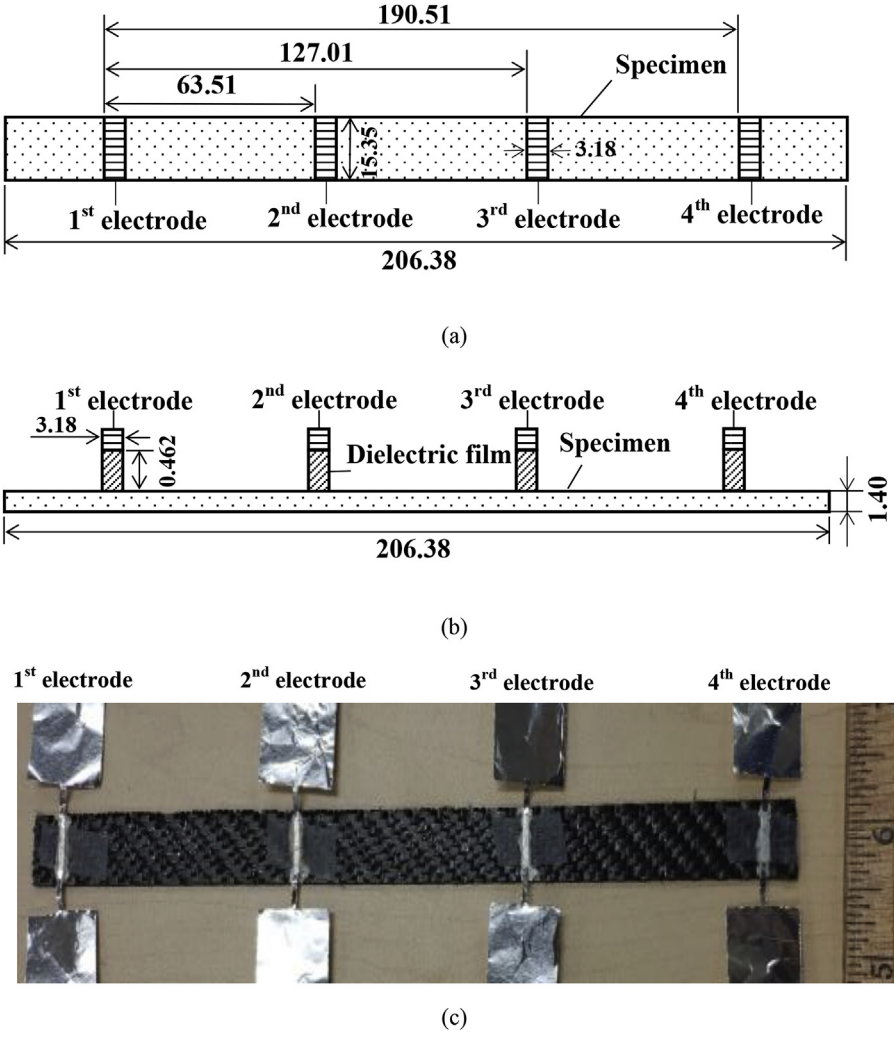

Fig. 2. Specimen configuration for measuring the relative permittivity of the carbon-carbon composite. All dimensions are in mm. Representative dimension values are shown. (a) Top view. (b) Side view. (c) Optical photograph of the specimen (vertical) with four electrodes, along with a ruler (horizontal) with major divisions in inches. The specimen thickness is 1.4 mm. In (b), the vertical scale in not the same as the horizontal scale.

the capacitance measurement is ±0.0005 pF. The capacitance reported is that for the equivalent circuit of capacitance and resistance in series. This circuit model is intended to indicate the setting used in the meter, rather than the method of analysis. The voltage (0.300, 0.600 or 0.900 V) is adjusted so that the electric field (4.724 V/m) is the same for different distances between the electrodes.

For measurement using each pair of electrodes, the two interfacial capacitances (for the two specimen-electrode interfaces) and the specimen volumetric capacitance are three capacitors in series electrically. Hence, the measured capacitance C_m is given by

$$1/C_m = 1/C + 2/C_i, \quad (7)$$

Where C is the specimen volumetric capacitance, and C_i is the interfacial capacitance for one interface. The C relates to κ of the specimen by the equation

$$C = \varepsilon_o \kappa A/l, \quad (8)$$

Where ε_o is the permittivity of free space (8.85×10^{-12} F/m), A is the area of the specimen in the plane perpendicular to the direction of capacitance measurement, and l is the length of the specimen between the two electrodes in the direction of the capacitance measurement (i.e., L, $2L$ or $3L$). Combining Eqs. (7) and (8) gives

$$1/C_m = l/(\varepsilon_o \kappa A) + 2/C_i. \quad (9)$$

Based on Eq. (9), a plot of $1/C_m$ vs. l gives a line of slope equal to $1/(\varepsilon_o \kappa A)$. Hence, from the slope, κ is obtained.

3.4. Electric field output measurement method

The voltage output of the direct piezoelectric effect is measured using the specimen configuration illustrated in Fig. 3, except that

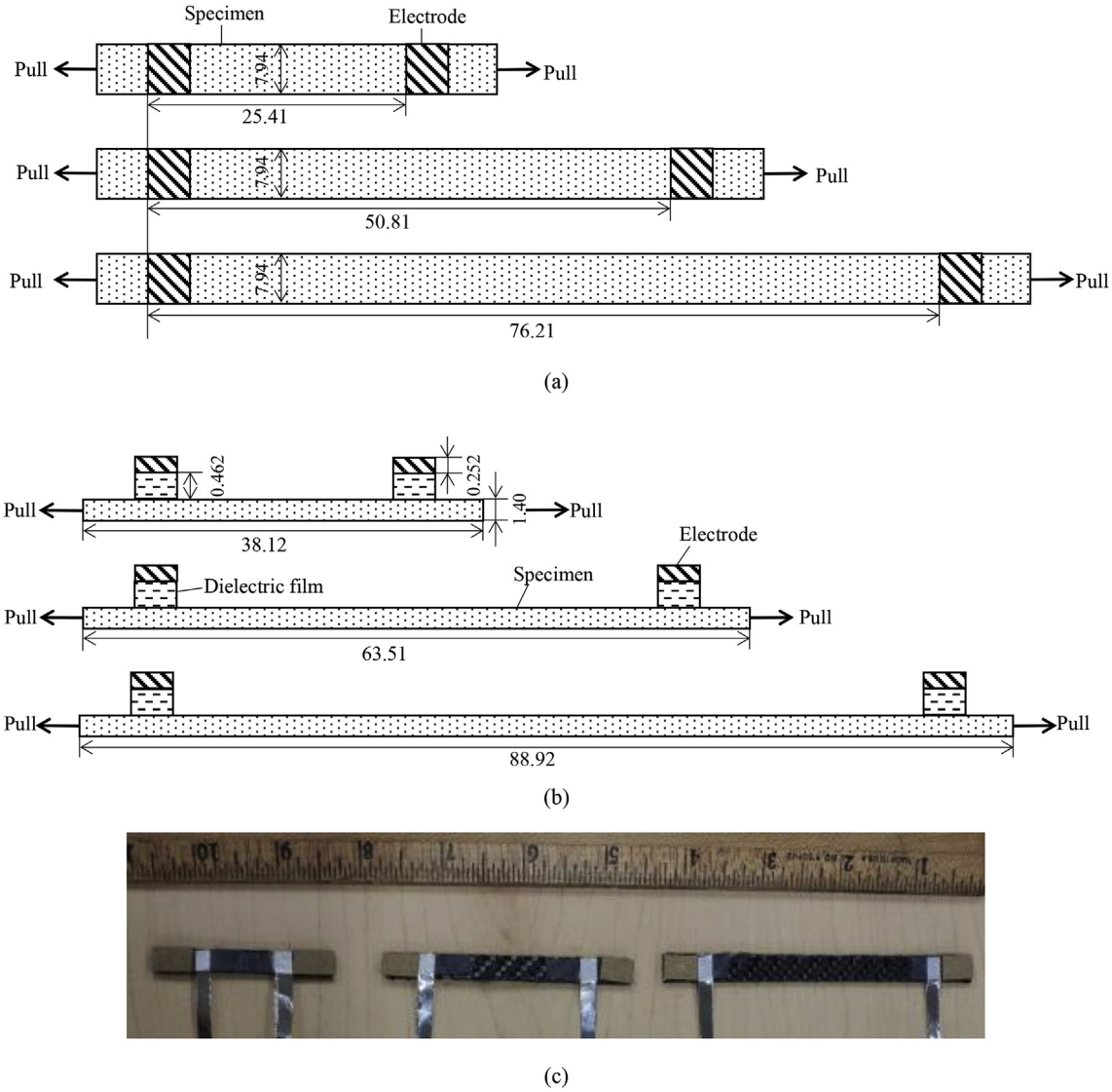

Fig. 3. Specimen configuration for characterizing the direct piezoelectric behavior of the carbon-carbon composite. The specimen thickness is 1.4 mm. All dimensions are in mm. Representative dimension values are shown. The configuration for measuring the electrical resistivity and electric field is the same except for the replacement of the dielectric film with silver paint. (a) Top view. (b) Side view. (c) Optical photograph of the specimens of three lengths (horizontal) with two electrodes for each specimen, along with a ruler (horizontal) with major divisions in inches. In (b), the vertical scale in not the same as the horizontal scale.

the dielectric film (used for capacitance measurement) is replaced by silver paint. The DC voltage is measured using a precision digital multimeter (Keithley Model 2002). For the relevant voltage range (within 200 mV), the resolution is 1 nV and the input resistance exceeds 100 GΩ [36]. The electric field is the voltage divided by the distance between the center lines of the electrodes. This distance is 2 L−50.81 mm, with the exact value measured for each specimen.

3.5. Resistivity measurement method

The DC electrical resistivity is measured using the specimen configuration illustrated in Fig. 3, except that the dielectric film (used for capacitance measurement) is replaced by silver paint. The method also involves the decoupling of the interfacial resistance from the volumetric resistance, as achieved by testing the fiber tow at three different lengths (L, 2 L and 3 L), where L ~ 25.41 mm, with the exact value measured for each specimen. In this context, the interface is that between the specimen and electrode, including the silver paint.

For measurement using two electrodes, the two interfacial resistances and the specimen volumetric resistance are three resistors in series electrically. Hence, the measured resistance R_m is given by

$$R_m = R + 2R_i, \tag{10}$$

Where R is the specimen volumetric resistance, and R_i is the interfacial resistance for one interface. The R relates to the resistivity ρ of the specimen by the equation

$$R = \rho l/A, \tag{11}$$

Where A is the area of the specimen in the plane perpendicular to the direction of resistance measurement, and l is the length of the specimen between the two electrodes (i.e., L, $2L$ or $3L$).

Combining Eqs. (10) and (11) gives

$$R_m = \rho l/A + 2R_i, \tag{12}$$

Based on Eq. (12), a plot of R_m vs. l gives a line of slope equal to ρ/A. Hence, from the slope, ρ is obtained.

The applied tensile stress of up to 4.83 MPa causes a tensile strain up to 8.1×10^{-5}, according to the modulus of 60 GPa. This strain causes the resistivity obtained by assuming zero strain at various stress values to be overestimated by up to 8.1×10^{-5}, which is negligible. The contribution due to the Poisson's effect is even more negligible.

The DC resistance is measured using a precision digital multimeter (Keithley Model 2002) operating in the two-wire mode. For the range of resistance of this work, the resolution is 100 nΩ and the current provided by the meter is 7.2 mA [36].

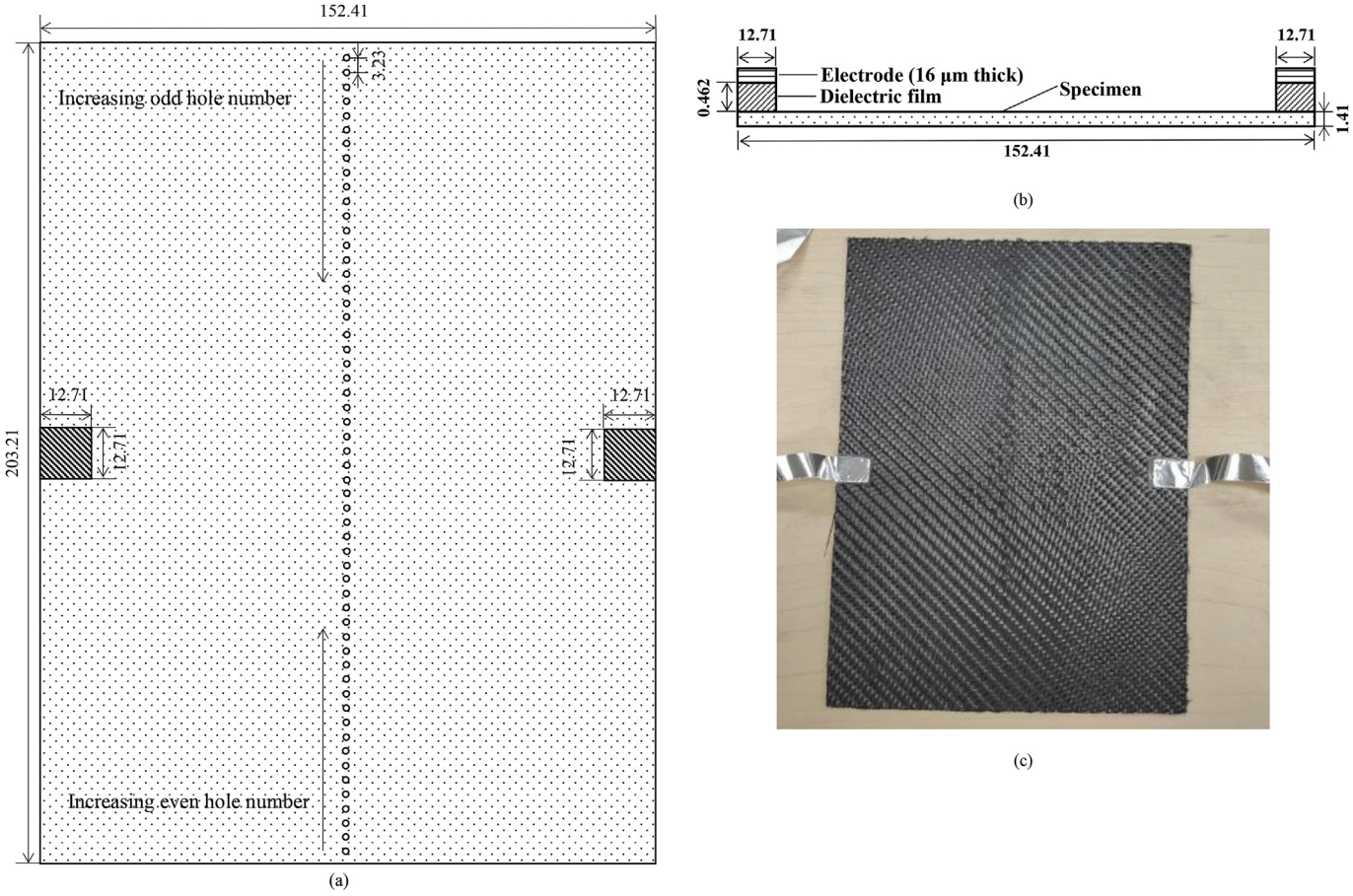

Fig. 4. (a) Testing configuration for capacitance measurement. The two coplanar electrodes are located on the same surface at the midpoints of two opposite 8-inch edges of the square specimen. All dimensions are in mm, unless noted otherwise. (a) Top view. Each hole is indicated by a solid circle. (b) Side view, with the vertical dimensions being exaggerated (not to scale). (c) Photograph of specimen. The row of holes is shown along a vertical line at the center of the photograph. The two electrodes in the form of aluminum foil are shown at the two sides.

3.6. NDE method

The apparent in-plane capacitance is measured by using two coplanar electrodes that are on the same surface of the specimen (Fig. 4). The electric field lines spread between the two electrodes. The intersection of the defects with the electric field lines causes the capacitance to change, relative to the case of no defect.

The frequency for the capacitance measurement is fixed. The method is in contrast to impedance spectroscopy [37–39], which involves measurement of the impedance (real and imaginary parts) as a function of the frequency and fitting the frequency dependence by using equivalent circuit models. Impedance spectroscopy suffers from the fact that the circuit models are not unique, so that the circuit parameters obtained by the curve fitting are not very meaningful scientifically. In addition, impedance spectroscopy suffers from the fact that measurement over a wide frequency range takes time and fast measurement is needed for real-time monitoring.

The electrodes are household aluminum foil. The dielectric film positioned between the electrode and the specimen is double-sided adhesive tape (6 layers stacked up, with each layer of thickness **77** μm), which also serves to adhere the electrode to the specimen. In practical implementation of this method, the dielectric film may be at least partly a dielectric coating (such as the oxidation protection coating) on the composite structure being evaluated. In other words, such coatings do not need to be removed prior to the application of the electrodes. In contrast, the removal of such coatings is needed if the resistance rather than the capacitance is measured.

An electrode (12.71 mm × 12.71 mm) in the form of aluminum foil is applied to the mid-point of each of two opposite 8-inch edges of the specimen, such that the outer edge of each square electrode coincides with an edge of the square specimen, as illustrated in Fig. 4. One of the two electrodes is grounded electrically.

The capacitance is measured using a precision LCR meter (Instek LCR-816). The frequency used is 2 kHz. The AC voltage is 1.275 V, which corresponds to an electric field of 10.04 V/m. The capacitance provided by the meter is for the meter setting in which the equivalent electrical circuit is that of a capacitance and a resistance in series.

3.7. Damage infliction and configuration

Damage in the form of (i) blind holes (1.00 mm diameter and 0.71 mm depth, with this depth including the tapered bottom of the blind hole) and (ii) through holes (1.4 mm depth) is artificially and manually inflicted at the same selected points, using the sharp end of a machining tool. The through holes are positioned at the same locations as the blind holes, all of which are formed before any of the through holes. The holes are positioned along a straight line at the center of the specimen, such that the line is perpendicular to the line joining the two electrodes and extends for the entire length of the specimen (Fig. 4). The number of holes is progressively increased from 1 to 62, so that the damage is cumulative. The holes are equally spaced, with the spacing being 3.23 mm. The holes are progressively closer and closer to the line joining the two electrodes. For each distance from the line joining the two electrodes, a hole is first formed at the distance on one side of the line joining the two electrodes and then a second hole is formed at the same distance on the opposite side of the line joining the two electrodes. In other words, there are two holes corresponding to each distance from the line joining the two electrodes. The hole configuration is illustrated in Fig. 4(a).

4. Results and discussion

4.1. Permittivity

The plot of $1/C_m$ vs. distance l according to Eq. (9) is highly linear, as shown in Fig. 5. The error in the relative permittivity κ is obtained by considering the range of values of the slope. Thus, $\kappa = 10743 \pm 1157$.

Table 1 shows that the relative permittivity of C/C is lower than but close to those of PAN-based carbon fiber [40] and aluminum [34]. Furthermore, it is higher than those of pitch-based carbon fibers [41], copper [35] and continuous carbon fiber polymer-matrix composite (CFRP) [27]. On the other hand, the resistivity of C/C is close to those of P-25 pitch-based carbon fiber and PAN-based carbon fiber, lower than those of CFRP, higher than those of pitch-based and PAN-based carbon fibers, and much higher than those of the metals (copper, aluminum, nickel, low carbon steel and stainless steel).

Both permittivity and resistivity are similar for C/C and the PAN-based carbon fiber [40]. This is consistent with the fact that the fibers in C/C are PAN-based. In spite of the large difference in resistivity between C/C and aluminum, the permittivity is similar between these two materials.

The permittivity of nickel-coated carbon fiber [42] is close to that of aluminum, though the resistivity is considerably higher for the nickel-coated carbon fiber. This reflects the dominance of the nickel coating in the nickel-coated carbon fiber is affecting the permittivity [42].

Comparison of CFRP, carbon fibers and C/C indicates that a lower resistivity tends to correlate with higher permittivity, though this correlation is not strong. Nevertheless, this correlation is consistent with the notion that a greater extent of electron movement promotes both conduction and polarization.

Comparison of the various metals in Table 1 indicates that higher resistivity correlates with higher permittivity. This means that, among metals, which have plentiful free electrons, the extent of electron movement does not govern the permittivity, but rather the ability of the material to sustain a higher electric field (as enabled by a higher resistivity) promotes the polarization.

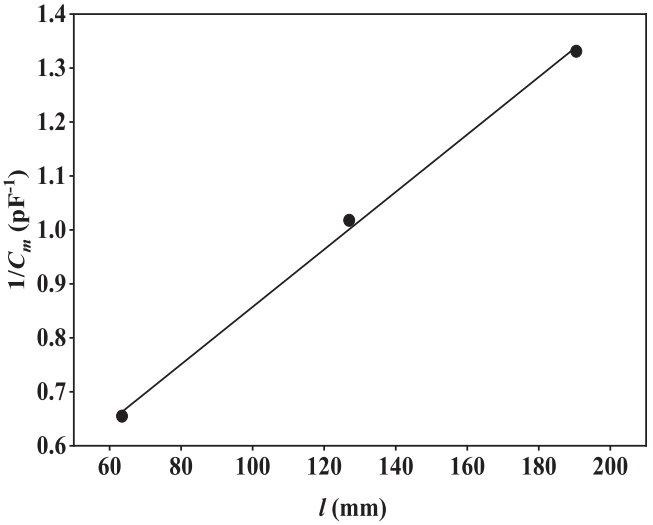

Fig. 5. Plot of $1/C_m$ vs. distance l according to Eq. (9) for stress = 0, as obtained using the configuration of Fig. 2.

Table 1
Relative permittivity (2 kHz) and electrical resistivity (DC) of various electrically conductive materials, listed in the order of increasing permittivity. CFRP: Carbon fiber reinforced polymer. C/C: Carbon-carbon composite. Carbon-based materials are indicated by italic font.

Material	Relative permittivity	Resistivity (Ω.cm)
CFRP (transverse) [27]	1.6×10^3	1.1×10^1
CFRP (longitudinal) [27]	2.2×10^3	7.2×10^{-3}
Copper [35]	2.4×10^3	1.4×10^{-6}
Carbon fiber (pitch-based, P-25) [41]	4.0×10^3	1.2×10^{-3}
Carbon fiber (pitch-based, P-100) [41]	5.0×10^3	1.8×10^{-4}
C/C (This work)	1.1×10^4	2.4×10^{-3}
Carbon fiber (PAN-based) [40]	1.2×10^4	1.6×10^{-3}
Aluminum [34]	5.5×10^4	2.7×10^{-6}
Nickel-coated carbon fiber [42]	6.3×10^4	1.5×10^{-5}
Nickel wire [42]	4.1×10^5	8.8×10^{-6}
Low carbon steel [43]	1.1×10^6	1.4×10^{-5}
Stainless steel [43]	2.3×10^6	7.2×10^{-5}

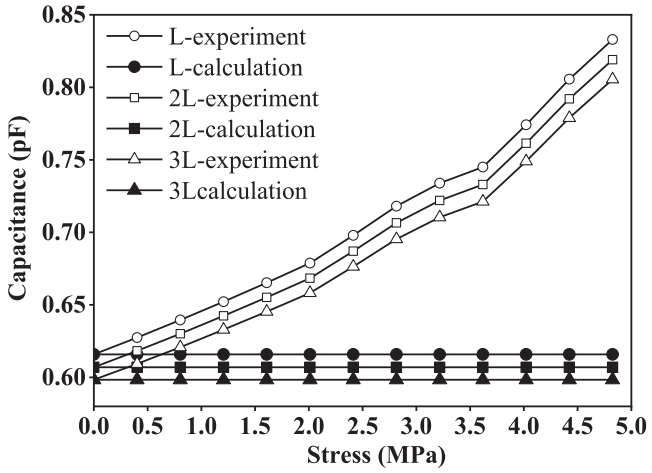

(a)

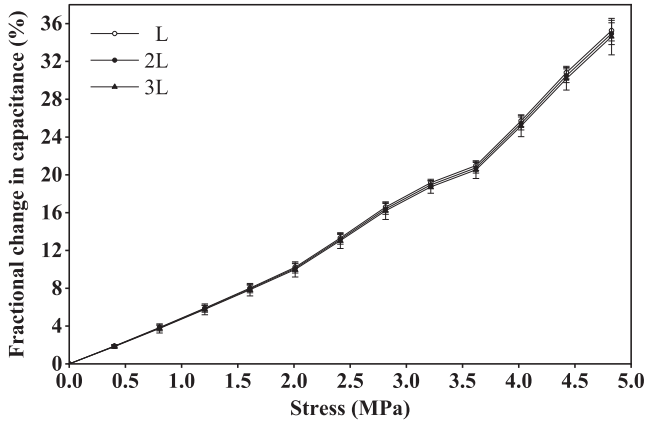

(b)

Fig. 6. Effect of tensile stress on the capacitance for lengths L, 2 L and 3 L, as obtained using the configuration of Fig. 3. (a) Capacitance, with comparison of the measured capacitance and calculated capacitance based on the dimensional changes. (b) Fractional change in the measured capacitance.

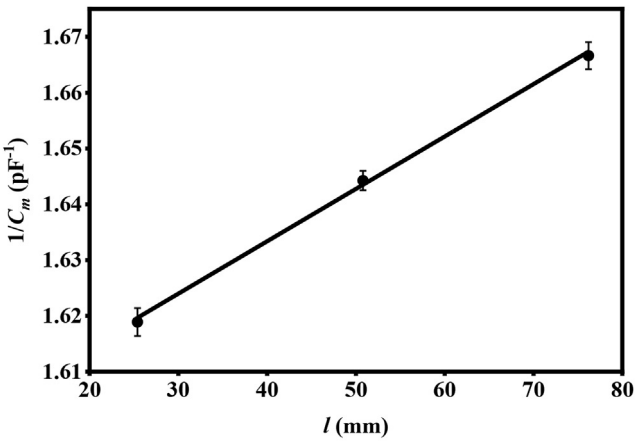

(a)

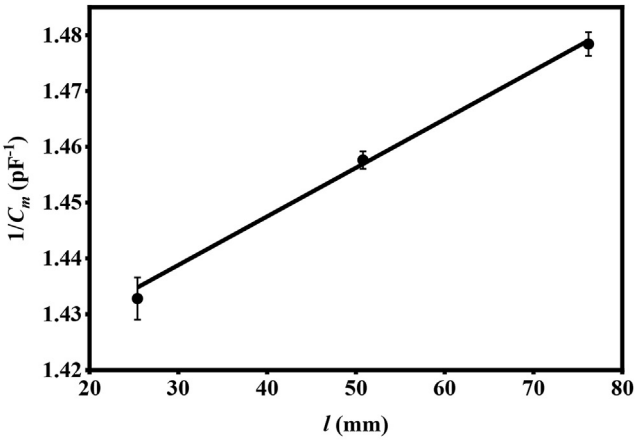

(b)

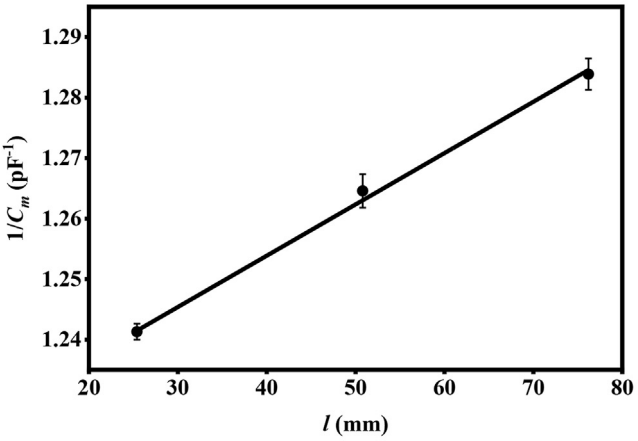

(c)

Fig. 7. Plot of $1/C_m$ vs. distance l according to Eq. (9) for various stress levels, as obtained using the configuration of Fig. 3. (a) 0 MPa. (b) 2.41 MPa. (c) 4.42 MPa.

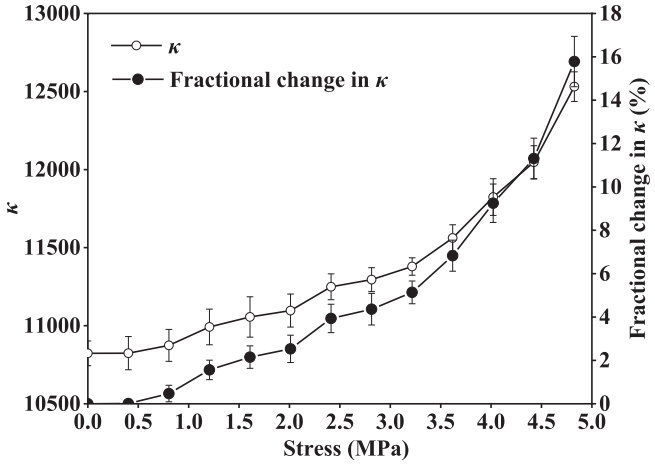

Fig. 8. Effect of stress on the relative permittivity κ, as obtained using the configuration of Fig. 3. For obtaining κ, the range of stress is from 0.4 to 2.8 MPa.

4.2. Effect of stress on the capacitance, permittivity and electric field

Fig. 6(a) shows that the capacitance increases monotonically with increasing tensile stress, whether the length is L, 2 L or 3 L. The fractional increase in capacitance (Fig. 6(b)) reaches 34% at the highest stress. The curves of the fractional increase in capacitance essentially overlap for the three lengths. Fig. 6(a) also shows that the calculated capacitance change based on the dimensional change alone is negligible compared to the measured capacitance change, indicating that the observed capacitance change is not due to the dimensional change, but is due to the direct piezoelectric effect. In fact, the tensile strain due to the stress is an elongation, which would cause the capacitance to decrease. In contrast, the observed capacitance change upon tension is an increase rather than a decrease.

Fig. 7 shows the plots of $1/C_m$ vs. distance l according to Eq. (9) for various stress levels, as obtained using the configuration of Fig. 3. The plot is linear for all stress levels. From the slope of each plot, the relative permittivity is obtained, as shown in Fig. 8. The relative permittivity increases monotonically with increasing stress. The fractional increase in relative permittivity reaches 16% at the highest stress. Fig. 9 shows that the increase in capacitance upon loading to the highest stress is reversible upon unloading.

Fig. 10 shows that the electric field decreases monotonically from 1.2×10^{-4} V/m to 9.1×10^{-5} V/m with increasing tensile stress. Furthermore, as shown in Fig. 10(b), the decrease is reversibly upon unloading from the highest stress. The electric field decrease upon tensile stress application (Fig. 10) occurs along with the relative permittivity increase (Fig. 8).

As shown in Table 2, the d_{33} value of C/C is negative based on Eq. (3), but is positive based on Eqs. (4) and (5). The magnitudes of the positive values are much smaller than that of the negative value. This means that the piezoelectric effect is dominated by the well-known piezoelectric effect involving the change in electric field due to the stress, and is negligibly contributed by the change of the relative permittivity with the stress.

Table 3 shows the comparison of the d_{33} value of C/C and those of low carbon steel and stainless steel. The d_{33} value of C/C is negative, like those of the steels. However, the magnitude of d_{33} is higher for the steels than C/C, partly due to the higher relative permittivity for the steels than C/C (Table 1). On the other hand, d_{33} is positive for carbon fiber, nickel-coated carbon fiber and nickel wire (Table 3). The positive value of nickel-coated carbon fiber has the same scientific origin as that the nickel wire. This means that the nickel coating of the nickel-coated carbon fiber dominates in affecting the d_{33} value. However, the positive d_{33} value of carbon fiber is in sharp contrast to the negative d_{33} value of C/C, even though both are carbons and they have similar values of the relative permittivity and resistivity (Table 1). This means that C/C and carbon fiber are opposite in the sign of the polarization that results from the same stress. Furthermore, the magnitude of d_{33} is much lower for C/C than the carbon fiber (Table 3), indicating that the magnitude of the polarization is much smaller for C/C than the carbon fiber. The density is 1.77 and 1.5 g/cm^3 for the carbon fiber and C/C, respectively. Thus, the low density of the carbon matrix of the C/C apparently hinders electron movement, thus reducing the polarization. The reverse polarization probably relates to the effect of stress on the orientation of the functional groups of both carbon fiber and carbon matrix and the interaction between the functional groups. The difference in d_{33} between C/C and carbon fiber is probably partly due to the difference in the strain range (Table 3). The strain is much higher for the carbon fiber than C/C. The scientific origin of the difference is not fully understood.

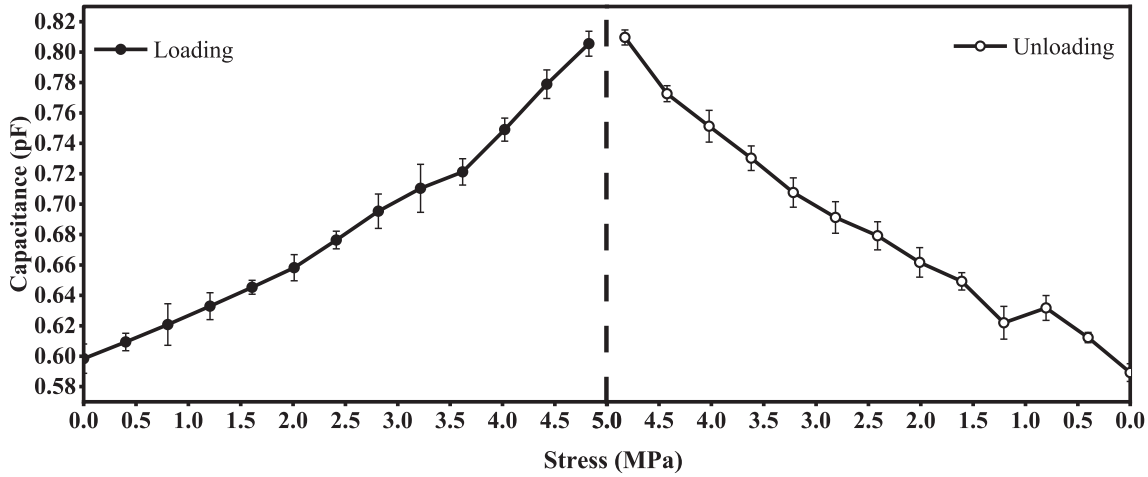

Fig. 9. Effect of stress on the capacitance during loading and subsequent unloading, as obtained using the configuration of Fig. 3, with the specimen length between the center lines of the two electrodes being 3 L = 76.21 mm. Left panel: loading. Right panel: unloading.

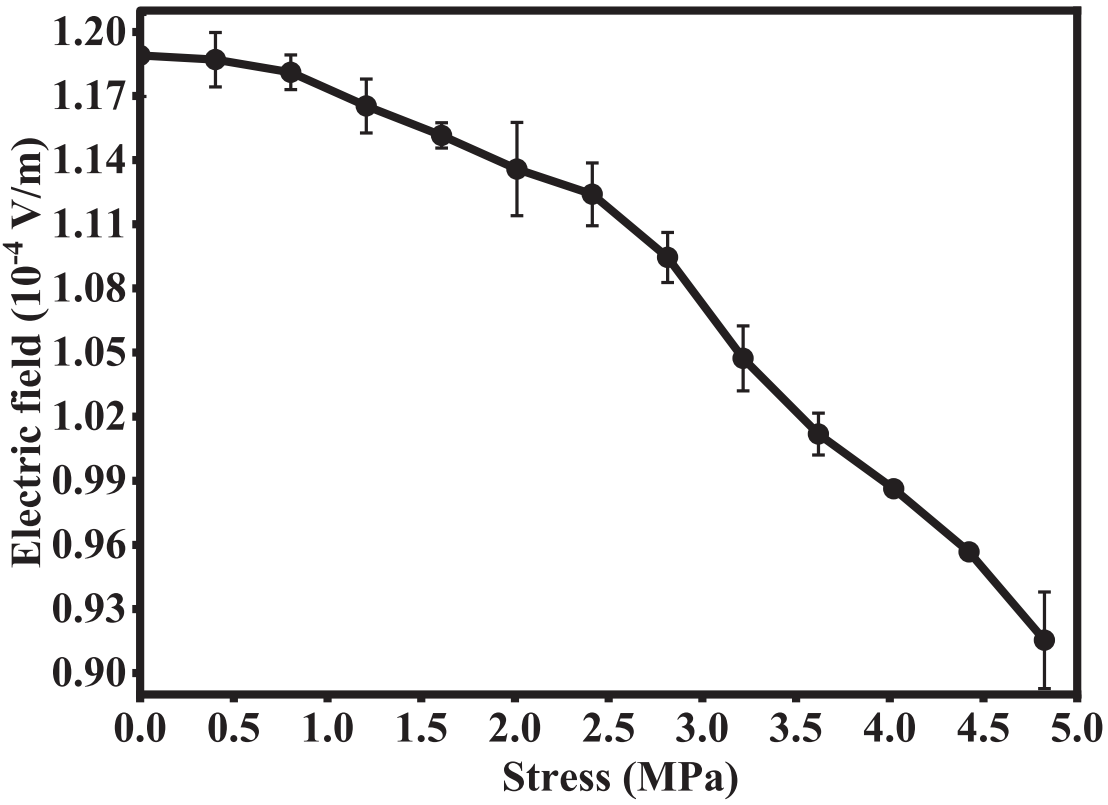

(a)

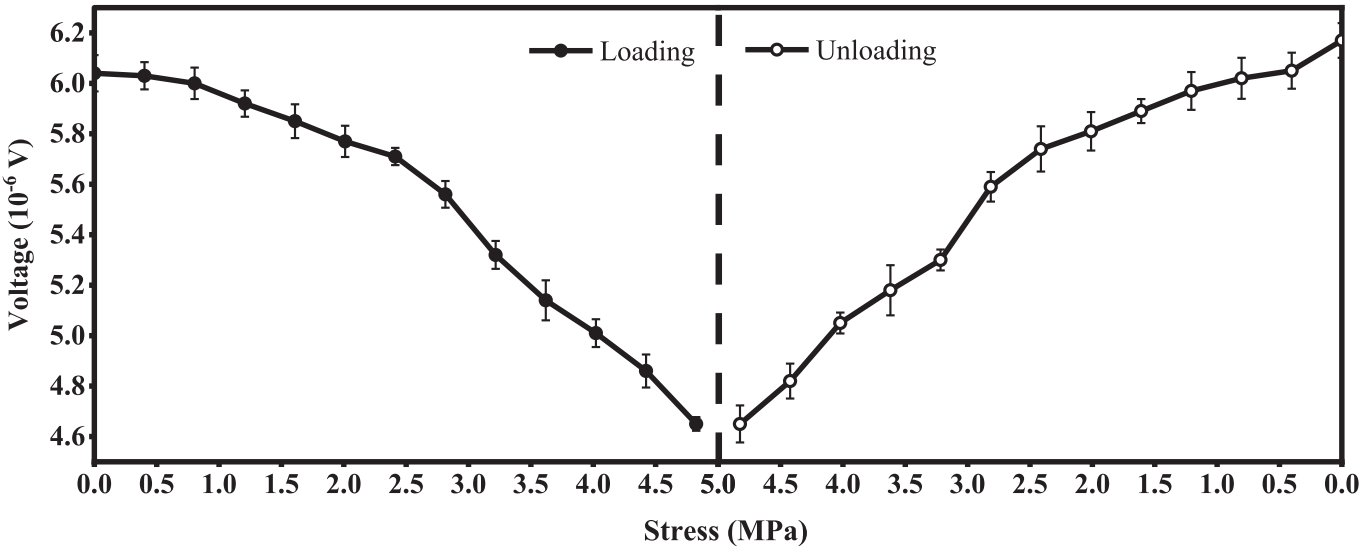

(b)

Fig. 10. Effect of stress on the electric field during loading, as obtained using the configuration of Fig. 3, with specimen length between the center lines of the two electrodes being 2 L = 50.81 mm. (a) Effect of stress on the electric field during loading. For obtaining the slope, the range of stress is from 2.81 to 4.82 MPa. (b) Effect of stress on the voltage during loading and subsequent unloading. Left panel: loading. Right panel: unloading.

Table 2
Piezoelectric coupling coefficient and gage factor of C/C. The stress/strain range is that for the relatively linear part of the associated curve. The strain is obtained from the stress and elastic modulus.

Property	Property value	Stress (MPa) range	Strain (%) range
d_{33} (pC/N), Eq. (3) [a]	$-(8.1 \pm 0.2) \times 10^{-9}$	2.81–4.82	0.0012–0.0020
d_{33} (pC/N), Eq. (4) [b]	$+(2.1 \pm 0.1) \times 10^{-14}$	0.40–2.81	0.0002–0.0012
d_{33} (pC/N), Eq. (5) [b]	$+(4.9 \pm 0.6) \times 10^{-15}$	0.40–2.81	0.0002–0.0012
Gage factor[c]	-7804 ± 429	0–2.01	0–0.00084

[a] Obtained from the slope of the designated relatively linear region of the curve of the electric field vs. stress.
[b] Obtained from the slope of the designated relatively linear region of the curve of the relative permittivity vs. stress.
[c] Obtained from the initial slope of the curve of resistivity versus stress.

Table 3
Piezoelectric coupling coefficient d_{33} and piezoresistive gage factor of carbons (italics) and metals. The strain is obtained from the stress and elastic modulus.

Material	d_{33} (pC/N)[a]	Stress (MPa) range for obtaining d_{33}	Strain (%) range for obtaining d_{33}	Gage factor	Stress (MPa) range for obtaining gage factor	Strain (%) range for obtaining gage factor
C/C (This work)	$-(8.1 \pm 0.2) \times 10^{-9}$	*2.81–4.82*	*0–0.00084*	*−7804 ± 429*	*0–2.01*	*0.0012–0.0020*
Carbon fiber (PAN-based) [40]	$+(1.7 \pm 0.3) \times 10^{-8}$	*25.71–60.39*	*0.0107–0.0252*	*−1830 ± 47*	*48.70–97.40*	*0.0203–0.0406*
Nickel-coated carbon fiber [42]	$+(5.6 \pm 0.2) \times 10^{-9}$	*8.49–59.43*	*0.00395–0.0276*	*+ 1651 ± 35*	*33.96–84.91*	*0.0158–0.0395*
Nickel wire [42]	$+(3.0 \pm 0.1) \times 10^{-9}$	89.53–223.81	*0.0439–0.109*	+30 ± 1	67.14–156.67	*0.0329–0.0768*
Low carbon steel [43]	$-(5.8 \pm 0.2) \times 10^{-8}$	170.17–283.61	*0.0851–0.142*	−1180 ± 97	226.89–321.43	*0.113–0.161*
Stainless steel [43]	$-(4.6 \pm 0.1) \times 10^{-8}$	56.72–283.61	*0.0284–0.142*	−984 ± 62	170.17–283.61	*0.0851–0.142*

[a] Based on Eq. (3).

4.3. Effect of stress on the resistance and resistivity

As shown in Fig. 11, the resistance decreases monotonically with increasing tensile stress for any of the three lengths (L, 2 L and 3 L). The fractional decrease in resistance due to the stress is essentially the same for the three lengths. Based on the changes in dimensions alone, the calculated resistance increases slightly with stress, as also shown in Fig. 11. Therefore, the observed significant resistance decrease is not due to dimensional changes, but is due to resistivity decrease.

The plot of R_m vs. distance l according to Eq. (12) is linear for any of the stress levels, as shown in Fig. 12 for three stress levels. The resistance decreases monotonically with increasing tensile stress and the decrease is reversible upon subsequent unloading, as shown in Fig. 13 for length = 3 L. Based on the slope of the plot of R_m vs. distance l (Fig. 12), the resistivity is obtained, as shown in Fig. 14. The fractional decrease in resistivity reaches 55% at the highest stress (Fig. 14(b)).

The resistivity decrease (Fig. 14) upon tensile stress application occurs along with the relative permittivity increase (Fig. 8). This is consistent with the notion that the movement of the electrons is responsible for both conduction and polarization. This correlation is consistent with the fact that CFRP in the longitudinal direction has lower resistivity and higher permittivity than CFRP in the transverse direction (Table 1).

Table 3 compares the gage factor of C/C with those of other materials. The gage factor is negative for C/C, carbon fiber, low carbon steel and stainless steel, but is positive for nickel-coated carbon fiber and nickel wire. The negative values of the gage factor are due to the preferred orientation increasing with the tensile stress, with the preferred orientation increase being reversible upon unloading, as shown by the reversibility of the resistance change [40,42]. The positive values of the gage factor, as obtained for nickel-coated carbon fiber and nickel wire [42], are due to the nickel (rather than the carbon) and probably result from the stress causing a reversible microstructural change that increases the resistivity. A example of a possible microstructural change is a change in the grain shape. However, the scientific origin is not fully

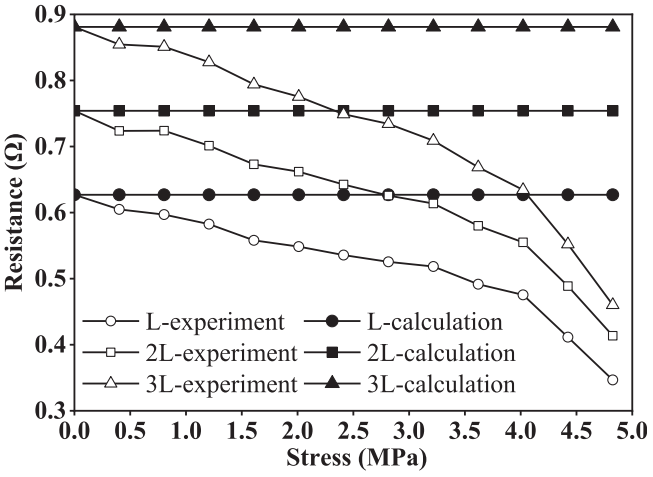

(a)

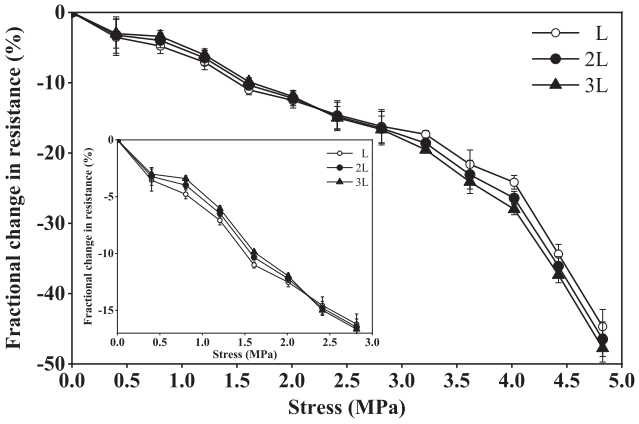

(b)

Fig. 11. Effect of stress on the electrical resistance during loading for lengths L, 2 L and 3 L, as obtained using the configuration of Fig. 3 (except for the dielectric film being replaced by silver paint). (a) Resistance. (b) Fractional change in resistance.

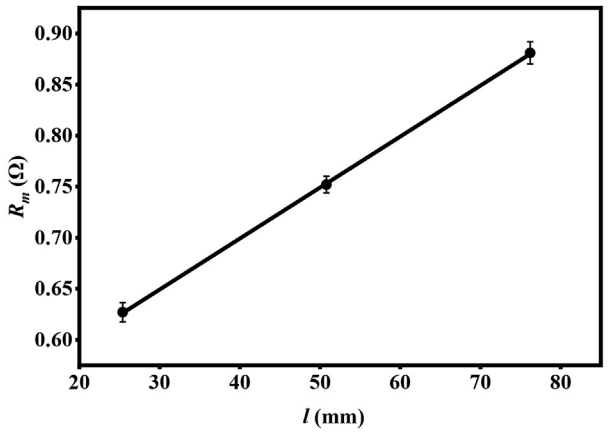

(a)

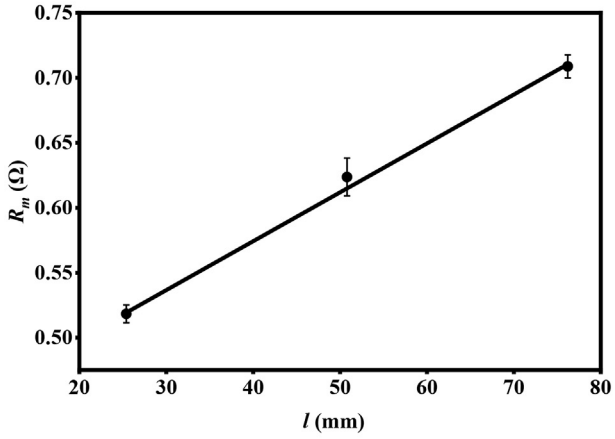

(b)

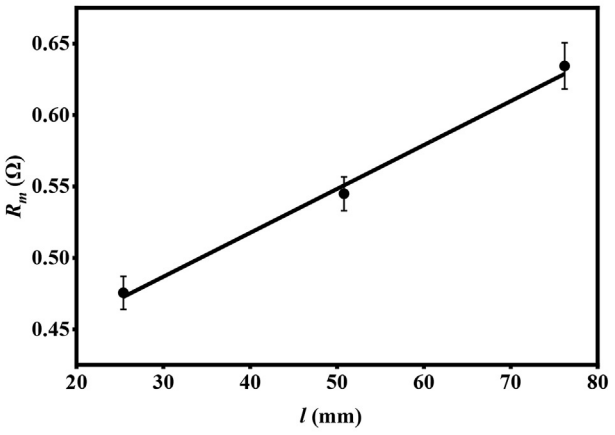

(c)

Fig. 12. Plot of R_m vs. distance l according to Eq. (12). (a) Stress = 0 MPa. (b) Stress = 3.22 MPa. (c) Stress = 4.02 MPa.

understood. The magnitude of the gage factor is roughly similar for the steels and carbon fiber, but is much higher for C/C, even though the resistivity is much lower for the steels than carbon fiber or C/C and the resistivity is similar for C/C and the carbon fiber (Table 1). Thus, the gage factor magnitude does not correlate with the resistivity. The much higher magnitude of the negative gage factor for C/C than the carbon fiber is probably due to low degree of preferred orientation in the carbon matrix of C/C, in contrast to the relatively high degree of preferred orientation in the carbon fiber. A lower degree of preferred orientation is expected to cause the stress to enhance the degree of preferred orientaton more strongly, particularly in the low-strain regime. However, the relatively high strain for the carbon fiber compared to C/C (Table 3) may contribute to casuing the difference in gage factor between the two materials.

In a previous study of a similar C/C, it was reported that the resistance increases monotonically with tensile strain ranging from 0.01% to 0.35%, with the gage factor ranging from +1.2 to +2.4 and the effect attributed mainly to dimensional changes rather than resistivity change [32]. In contrast, this work indicates strong negative piezoresistivity for strain up to 0.0081% and attributes the effect to the preferred orientation increasing with the tensile stress, as discussed above. The absence of the piezoresistivity effect at strains above about 0.01% is probably due to the saturation of the preferred orientation enhancement above a strain of about 0.01%. If the deformation were to occur at an elevated temperature instead of room temperature, the saturation would be expected to occur at a higher strain. The fact that the negative piezoresistivity was not observed in the prior work is also probably due to the strain in the experiment being not controlled well enough in the low strain regime below 0.01%.

4.4. NDE results

Fig. 15 shows the effect of damage on the measured capacitance. The capacitance decreases monotonically with increasing level of damage, whether the damage is in the form of blind holes or through holes. The capacitance decrease occurs beyond 12 blinds holes in the specimen, but occurs beyond 0 through hole, as shown by comparing the two panels in Fig. 15. As expected, the through holes affect the capacitance more than the blind holes. The capacitance decrease is attributed to the air in the holes having a low permittivity. This decreasing trend is the same as that previously reported by this research group for a continuous carbon fiber polymer-matrix composite [27] and aluminum [33], both with damage in the form of through holes and the capacitance similarly measured using coplanar electrodes.

The measured capacitance is governed by both the permittivity and resistivity (Table 1). The permittivity directly relates to the capacitance (Eq. (8)), while the resistivity governs the extent of current spreading. The quantitative relationship among the measured capacitance, permittivity and resistivity is yet to be obtained.

It was previously reported in a similar C/C that minor stress-induced damage is accompanied by an irreversible increase in the electrical resistance [32]. However, the effectiveness of the irreversible resistance increase as an indicator of damage like the through holes of this work has not been shown.

5. Conclusion

Capacitance-based nondestructive flaw detection, electric permittivity, piezoelectricity (capacitance-based stress self-sensing) and piezoresistivity (resistance-based stress self-sensing) of C/C (with PAN-based carbon fiber) are reported for the first time. The capacitance-based NDE is valuable for assessing the flaws after various numbers of densification cycles in the composite fabrication process, in addition to assessing the flaws after the entire fabrication process and after various extents of use.

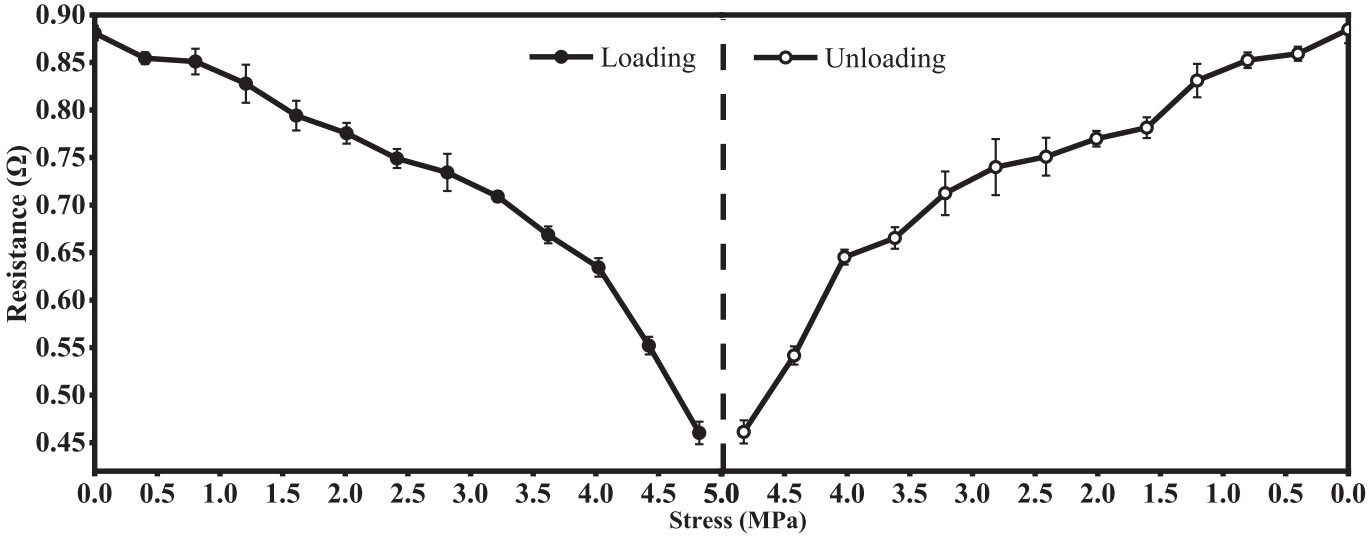

Fig. 13. Effect of stress on the electrical resistance during loading and subsequent unloading, with the specimen length between the center lines of the two electrodes being 3 L = 76.21 mm. Left panel: loading. Right panel: unloading.

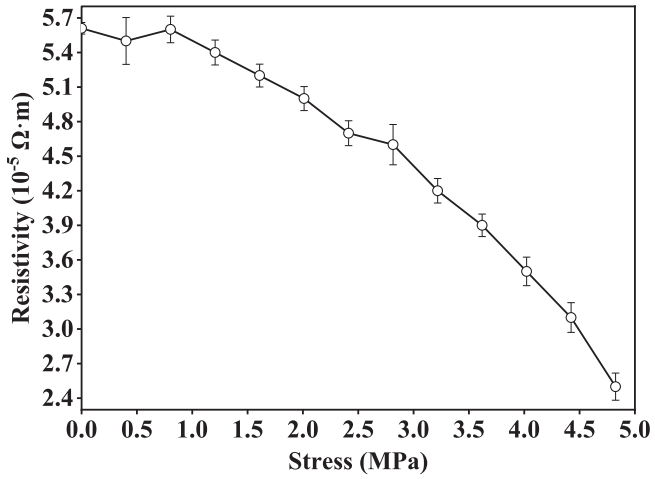

(a)

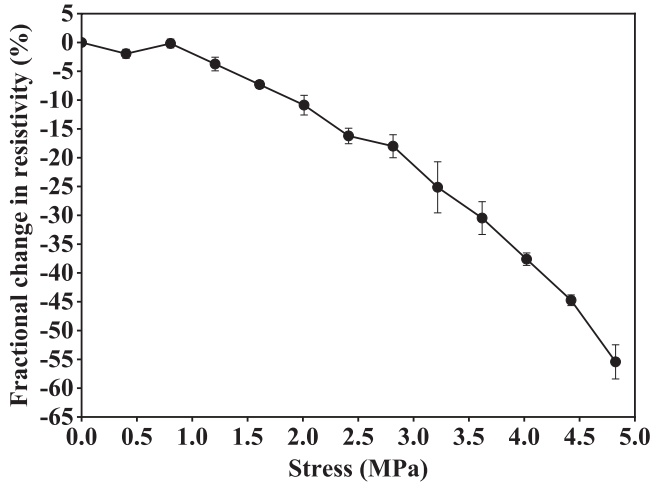

(b)

Fig. 14. Effect of tensile stress on the resistivity during loading. (a) Resistivity. For obtaining the slope, the range of stress is from 0 to 2.01 MPa. (b) Fractional change in resistivity.

The in-plane capacitance, measured using two coplanar electrodes that are much smaller in area than the specimen, decreases monotonically with increasing cumulative artificially inflicted damage in the form of holes of diameter 1.00 mm. The number of holes range from 1 to 62. The decrease is more when the number of holes is greater and is more for through holes than blind holes. This indicates the feasibility of capacitance-based nondestructive evaluation of C/C. The positioning of a dielectric film between the electrode and C/C is necessary for the effective use of the LCR meter.

The in-plane relative permittivity is 1.1×10^4 at 2 kHz and the in-plane DC resistivity is $2.4 \times 10^{-3}\,\Omega$.cm, as measured with decoupling of the volumetric and interfacial contributions. These values are similar to those previously reported for PAN-based carbon fiber [20]. The permittivity is higher and the resistivity is lower than those of CFRP in the longitudinal direction.

The relative permittivity increases reversibly by up to 16% with increasing tensile strain (up to 0.0081%). However, the contribution of the stress-dependent permittivity to the piezoelectric effect is negligibly small. The observed direct piezoelectric effect is primarily due to the reversible monotonic decrease of the in-plane electric field output from 1.2×10^{-4} V/m to 9.1×10^{-5} V/m with increasing tensile strain (up to 0.0081%).

The in-plane piezoelectric coupling coefficient d_{33} (for tensile strain up to 0.0081%) is negative, with value $-(8.1 \pm 0.2) \times 10^{-9}$ pC/N, which is in contrast to the higher-magnitude positive value of $+(1.7 \pm 0.3) \times 10^{-8}$ pC/N for the PAN-based carbon fiber [40]. In spite of the low magnitude of d_{33}, the piezoelectricity enables stress self-sensing through measurement of the capacitance or electric field.

The in-plane piezoresistivity gage factor (for tensile strain up to 0.0081%) is negative, with value -7804 ± 429, which is much higher in magnitude than the negative value of -1830 ± 47 previously reported for the PAN-based carbon fiber [40]. The high magnitude of the gage factor of C/C is attractive for resistance-based stress self-sensing.

The differences in d_{33} and gage factor between C/C and the PAN-based carbon fiber are attributed mainly to the carbon matrix in the C/C. Due to its relatively low crystallographic order and low density compared to the fiber itself, the carbon matrix responds to stress differently from the carbon fiber.

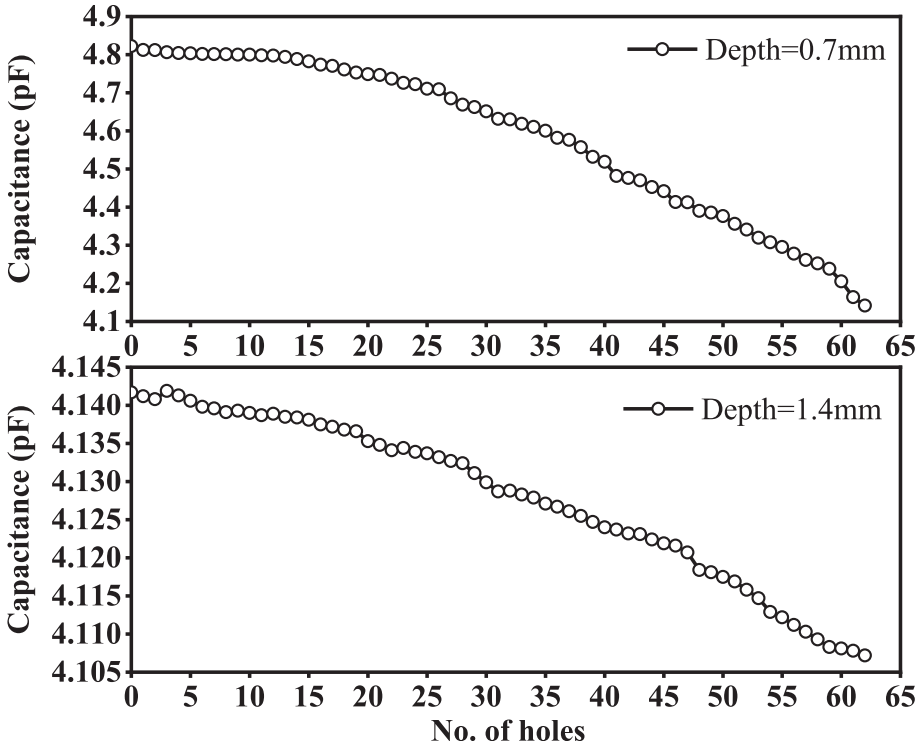

Fig. 15. Effect of the number of holes in the specimen on the measured capacitance. Top panel: blind holes of depth 0.7 mm. Bottom panel: through holes of depth 1.4 mm.

References

[1] D.D.L. Chung, Carbon Composites, second ed., Elsevier, 2016. Ch. 7.
[2] A.V. Nasibulin, E.A. Antipov, N.Y. Beilina, G.S. Dogadin, N.A. Makarov, Effect of modifying pitch on carbon-carbon composite material density, Refract. Ind. Ceram. 58 (1) (2017) 74–77.
[3] X. Lu, Z. Jie, K. Qian, Densification rate and mechanical properties of carbon/carbon composites with layer- designed preform, Ceram. Int. 45 (4) (2019) 4167–4175.
[4] T.S.K. Raunija, Influence of temperature and time shifts on the densification of randomly oriented carbon/carbon composite, Def. Sci. J. 65 (5) (2015) 411–417.
[5] W. Chen, Numerical analyses of ablative behavior of C/C composite materials, Int. J. Heat Mass Tran. 95 (2016) 720–726.
[6] M. Bevilacqua, A. Babutskyi, A. Chrysanthou, A review of the catalytic oxidation of carbon- carbon composite aircraft brakes, Carbon 95 (2015) 861–869.
[7] A.A. SDtepashkin, D.Y. Ozherelkov, Y.B. Sazonov, A.A. Komissarov, V.V. Mozolev, Assessment of fracture toughness of a discretely- reinforced carbon- carbon composite material, Met. Sci. Heat Treat. 57 (3–4) (2015) 229–235.
[8] Y. Chen, S. Xiao, H. Chen, H. Liu, The effect of catalyzer in the matrix on the structure and performance of carbon/carbon composite, J. Compos. Mater. 47 (4) (2013) 409–417, 10.
[9] A. Wang, D.D.L. Chung, First report of fumed alumina incorporation in carbon-carbon composite and the consequent improvement of the oxidation resistance and mechanical properties, Carbon 101 (2016) 281–289.
[10] S. Biwa, K. Nagae, C. Inserra, E. Matsumoto, Evaluation of nonlinear low-frequency components generated by amplitude- modulated waves in a carbon/carbon composite, AIP Conf Proc 1433 (2012) 497–500 (International Congress on Ultrasonics, 2011).
[11] I. Yang, Y. Kim, J. Park, D.K. Hsu, S. Song, H. Cho, S. Kim, K. Im, Airborne ultrasonic inspection in carbon/carbon composite materials, Proc. SPIE (2007) 6423 (Pt. 2, Int Conf Smart Mater Nanotechnol Eng, 2007):64232W/1-64232W/7.
[12] A. Bussiba, R. Piat, M. Kupiec, R. Carmi, I. Alon, T. Boehlke, Damage onset and growth in carbon carbon composite monitored by acoustic emission technique, J Acoustic Emission 27 (2009) 77–88.
[13] M.Z. Umar, V.P. Vavilov, H. Abdullah, A.K. Ariffin, Detecting low-energy impact damages in carbon- carbon composites by ultrasonic infrared thermography, Russian J Nondestructive Testing 53 (7) (2017) 530–538.
[14] J. Liu, Y. Wang, Experimental study on active infrared thermography as a NDI tool for carbon- carbon composites, Composites, Part B 45 (1) (2013) 138–147.
[15] Y.P. Pan, T.P. Chu, P. Filip, Intelligent nondestructive testing expert system for carbon- carbon composites using infrared thermography, Mater Evaluation 69 (7) (2011) 834–842.
[16] J. Liu, Q. Tang, Y. Wang, The study of inspection on SiC coated carbon- carbon composite with subsurface defects by lock-in thermography, Compos. Sci. Technol. 72 (11) (2012) 1240–1250.
[17] Q. Tang, J. Liu, Y. Wang, L. Qi, Q. Lei, Inspection on SiC coated carbon- carbon composite with subsurface defects using pulsed thermography, Infrared Phys. Technol. 60 (2013) 183–189.
[18] G.L. Vignoles, O. Coindreau, A. Ahmadi, D. Bernard, Assessment of geometrical and transport properties of a fibrous C/C composite preform as digitized by X-ray computerized microtomography: part II. Heat and gas transport properties, J. Mater. Res. 22 (6) (2007) 1537–1550.
[19] J.N. Perie, H. Leclerc, S. Roux, F. Hild, Digital image correlation and biaxial test on composite material for anisotropic damage law identification, Int J Solids Structures 46 (11–12) (2009) 2388–2396.
[20] X. Wang, S. Wang, D.D.L. Chung, Sensing damage in carbon fiber and its polymer-matrix and carbon-matrix composites by electrical resistance measurement, J. Mater. Sci. 34 (11) (1999) 2703–2714.
[21] Li-Zhen Xue, Ke-Zhi Li, Shou-Yang Zhang, He-Jun Li, Jing Cheng, Wen-Fei Luo, Monitoring the damage evolution of flexural fatigue in unidirectional carbon/carbon composites by electrical resistance change method, Int. J. Fatig. 68 (2014) 248–252.
[22] D.D.L. Chung, Functional Materials, World Scientific Pub, 2010 (Chapter 2).
[23] S. Wang, D.S. Pang, D.D.L. Chung, Hygrothermal stability of electrical contacts made from silver and graphite electrically conductive pastes, J. Electron. Mater. 36 (1) (2007) 65–74.
[24] C. Leong, D.D.L. Chung, Pressure electrical contact improved by carbon black paste, J. Electron. Mater. 33 (3) (2004) 203–206.
[25] X. Luo, D.D.L. Chung, Graphite-graphite electrical contact under dynamic mechanical loading, Carbon 39 (2001) 615–618.
[26] X. Luo, D.D.L. Chung, Material contacts under cyclic compression, studied in real time by electrical resistance measurement, J. Mater. Sci. 35 (19) (2000) 4795–4802.
[27] A.A. Eddib, D.D.L. Chung, First report of capacitance-based self-sensing and in-plane electric permittivity of carbon fiber polymer-matrix composite, Carbon 140 (2018) 413–427.
[28] X. Hong, W. Yu, D.D.L. Chung, Electric permittivity of reduced graphite oxide, Carbon 111 (2017) 182–190.
[29] D.D.L. Chung, Processing-structure-property relationships of continuous carbon fiber polymer-matrix composites, Mater. Sci. Eng. R 113 (2017) 1–29.
[30] D.D.L. Chung, Functional Materials, World Sci Pub, 2010. Chapters 2 and 3.
[31] M.S. Aly-Hassan, H. Hatta, S. Wakayama, M. Watanabe, K. Miyagawa, Comparison of 2D and 3D carbon/carbon composites with respect to damage and fracture resistance, Carbon 41 (5) (2003) 1069–1078.
[32] S. Wang, D.D.L. Chung, Self-monitoring of strain and damage by a carbon-carbon composite, Carbon 35 (5) (1997) 621–630.

[33] D.D.L. Chung, K. Shi, Sensing the stress in steel by capacitance measurement, Sensor. Actuator. A274 (2018) 244–251.
[34] X. Xi, D.D.L. Chung, Piezoresistivity, piezoelectricity and dielectricity discovered in aluminum, with relevance to structural self-sensing. Sens. Actuators A. (in press).
[35] X. Xi, D.D.L. Chung, Piezoelectricity, piezoresistivity and dielectricity discovered in copper. (submitted for publication).
[36] https://xdevs.com/doc/Keithley/2002/SPEC-2002.pdf (as viewed on Sept. 22, 2018).
[37] E. Sentuerk, M. Okutan, S.E. San, O. Koeysal, Debye type dielectric relaxation in carbon nano-balls' and 4-DMAABCA acid doped E7 coded nematic liquid crystal, J. Non-Cryst. Solids 354 (30) (2008) 3525–3528.
[38] P. Xie, W. Sun, Y. Liu, A. Du, Z. Zhang, G. Wu, R. Fan, Carbon aerogels towards new candidates for double negative metamaterials of low density, Carbon 129 (2018) 598–606.
[39] P. Xie, Z. Zhang, K. Liu, L. Qian, F. Dang, Y. Liu, R. Fan, X. Wang, S. Dou, C/SiO_2 meta-composite: overcoming the λ/a relationship limitation in metamaterials, Carbon 125 (2017) 1–8.
[40] X. Xi, D.D.L. Chung, Colossal electric permittivity discovered in polyacrylonitrile (PAN) based carbon fiber, with comparison of PAN-based and pitch-based carbon fibers, Carbon 145 (2019) 734–739.
[41] A.A. Eddib, D.D.L. Chung, Electric permittivity of carbon fiber, Carbon 143 (2019) 475–480.
[42] X. Xi, D.D.L. Chung, Effect of nickel coating on the stress-dependent electric permittivity, piezoelectricity and piezoresistivity of carbon fiber, with relevance to stress self-sensing, Carbon 145 (2019) 401–410.
[43] X. Xi, D.D.L. Chung, Piezoelectricity and piezoresistivity in unmodified steels, with relevance to structural self-sensing. (submitted for publication).